Integrated electromagnetic actuator with adaptable zero power gravity compensation

Alexander Pechhacker, Daniel Wertjanz, Ernst Csencsics, and Georg Schitter, *Senior Membership, IEEE*

***Abstract*—This paper presents a novel integrated electromagnetic actuator with a position-independent zero power gravity compensation mechanism for variable masses. Gravity is actively compensated by a variable reluctance actuator with a seamlessly tunable electropermanent magnet. To counteract the negative stiffness of the variable reluctance actuator, Lorentz actuators are used to stabilize the position of a magnetically levitated mover in two DoFs. A local search algorithm tunes the EPM, providing a variable force between 0 and 25 N. Experimental results demonstrate a reduction of the power consumption by at least four orders of magnitude in comparison to the purely Lorentz actuated system and a gravity compensation tuning rate of 2.6 N/s, verifying the utilization of the actuator for energy efficient positioning systems or vibration isolation systems with variable effective loads.**

***Index Terms*—Actuators, Electromagnetic forces, Mechatronics.**

I. Introduction

GRAVITATIONAL forces need to be compensated in various industrial applications, ranging from nanopositioning systems for the semiconductor industry [1], [2] to conventional magnetic bearings [3], vibration isolation systems [4], potential energy storage [5] and sample tracking platforms for robot-based inline measurement systems [6].

Lorentz actuators (LAs) are widely used in high-performance mechatronic systems due to their linearity and zero-stiffness [7]. A major drawback of purely LA-based gravity compensation is the offset current in the coils, resulting in a stationary power consumption [8]. The dissipated power increases the temperature, which may cause a decreased precision of the entire system [9]. Moreover, the maximum coil current available for generating dynamic forces is reduced by the offset current, limiting the dynamic range and achievable performance of a positioning system or a vibration isolation system.

Various design approaches to achieve the desired zero power gravity compensation are based on the attractive and repulsive forces of permanent magnets [10], [11]. By adapting the mover position according to the effective mass, the system can be kept in a force equilibrium operating point. This approach is further optimized by increasing the compensating force with Halbach arrays [12]. Another design with two degrees of freedom (DoFs) is based on the principle of a hybrid reluctance actuator (HRA) [13]. The negative stiffness of the HRA is also utilized to generate a position-dependent compensation force. However, all reported approaches based on permanent magnets compensate gravity by vertically adapting the mover position according to the mover mass. To solve this problem, a system with adjustable displacements between permanent magnets and mover is introduced [14], enabling variable compensation forces. The permanent magnets are actuated by thermal shape memory actuators for energy efficiency, but they limit the bandwidth of the gravity compensation mechanism to around $10\,\mathrm{mHz}$.

Compared to permanent magnets, conventional electropermanent magnets (EPMs) have the ability to switch the remanent magnetic flux on (maximum magnetic flux) and off (no magnetic flux) while the static power is zero [15]. This bi-stable mechanism is suitable for switchable reluctance actuators with holding forces from $145\,\mathrm{kN}$ to $1\,\mathrm{mN}$ [16], [17], stepper motors [15], microfluidic valves [18] or climbing robots [19]. Reluctance actuators based on EPMs and operated in the static on and off state could be used for a switchable gravity compensation, but would still have the disadvantage of the position-dependent gravity compensation force.

The contribution of this paper is the design of an integrated electromagnetic actuator (IEA) with an adaptable gravity compensation mechanism, which enables magnetic levitation of a variable mass in a desired position at zero static power consumption. A control strategy for a tuneable permanent magnet to adapt the gravity compensation force according to the mover mass, as well as a position control to stabilize the mass at a desired position are developed. The system performance is evaluated and the significantly reduced static power consumption is successfully demonstrated on an experimental setup.

II. System concept and requirements

The system concept is centered around a variable reluctance actuator with a tunable permanent magnet, as shown in Fig. 1. Current pulses in the enveloping magnetization coil are utilized to magnetize the permanent magnet, generating an adaptable magnetic flux in the air gaps between mover and stator. The changing magnetic flux results in a tunable reluctance force $F_{PM}(t)$ at a desired mover position. By tuning the reluctance

Manuscript received 24 October 2022; revised 5 June 2023; accepted 15 June 2023. The financial support by the Christian Doppler Research Association, the Austrian Federal Ministry for Digital and Economic Affairs, and the National Foundation for Research, Technology and Development are gratefully acknowledged.

The authors are with the Advanced Mechatronic Systems (AMS) group at the Automation and Control Institute (ACIN), Technische Universität Wien, 1040 Vienna. Corresponding author: pechhacker@acin.tuwien.ac.at

Post-print version of the article: A. Pechhacker, D. Wertjanz, E. Csencsics, and G. Schitter, "Integrated electromagnetic actuator with adaptable zero power gravity compensation," *IEEE Transactions on Industrial Electronics*, Early Access, 2023. DOI: 10.1109/TIE.2023.3288176

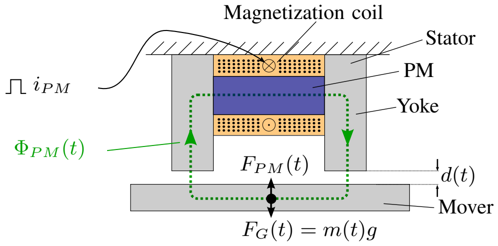

Fig. 1: Concept of a variable reluctance actuator with a tunable permanent magnet. The permanent magnet generates a quasi-static magnetic flux $\Phi_{PM}(t)$ that can be adapted by the current in the magnetization coil. The variable flux $\Phi_{PM}(t)$ is used to compensate the gravitational forces $F_G(t)$.

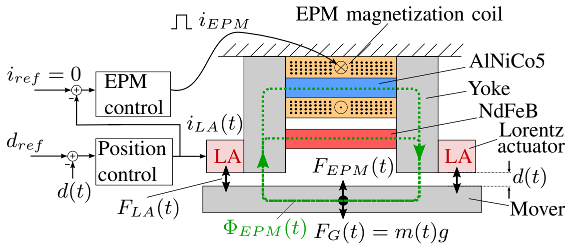

Fig. 2: System concept of the IEA. The EPM generates a flux Φ_{EPM} that attracts the mover and the integrated LAs stabilize the mover position $\boldsymbol{d}$. Using the Lorentz coil currents $\boldsymbol{i}_{LA}$, the EPM controller compensates the gravitational forces F_G of the mover.

force to compensate the gravitational force of the mover mass $F_{PM}(t) = F_G(t)$, the mover is magnetically levitating without power consumption. If the mover mass $m(t)$ is changed or the actuator orientation with respect to the gravity vector is modified [20], the reluctance force is retuned to compensate the corresponding gravitational force.

The tunable permanent magnet is realized by an EPM to reduce the volume of the magnetic material which is magnetized, resulting in reduced hysteresis losses while adapting the reluctance force [15]. An EPM consists of a hardmagnetic NdFeB and semi-hardmagnetic AlNiCo material with equal cross-sections and remanence, shown in Fig. 2. By applying current pulses to an enveloping coil, the magnetization of the AlNiCo material can be changed. In this way, the magnetic fluxes of both magnets either compensate each other or add up, yielding a permanent magnet with the magnetic flux only in one orientation. In contrast to the state of the art, the EPM is seamlessly tuned in the range between off (no magnetic flux) and on state (maximum magnetic flux).

The negative stiffness acting in each air gap of the variable reluctance actuator entails an unstable equilibrium position ($F_{EPM}(t) = F_G(t)$). Due to the unstable equilibrium position, additional actuators need to be integrated to provide a stabilizing force in two DoFs. Based on the desirable linearity and zero-stiffness, LAs are chosen to be integrated. Figure 2 shows the system concept of the IEA, that combines a tunable reluctance actuator for gravity compensation and two LAs to stabilize the mover position.

The cascaded control design for the IEA is separated in the inner position control loop and the outer EPM control loop, shown in Fig. 2. The position control stabilizes the desired mover position $\boldsymbol{d}_{ref}(t)$ via the LAs. The currents in the LAs $i_{LA}(t)$ are in a linear relation to the Lorentz force $\boldsymbol{F}_{LA}(t)$. Therefore the currents in the LAs identify the deviation from the force equilibrium, in which $F_{EPM}(t) = F_G(t)$ and $F_{LA}(t) = 0$. The outer EPM control tunes the magnetic flux of the EPM and the resulting reluctance force $F_{EPM}(t)$ with magnetization current pulses $i_{EPM}(t)$ to obtain the force equilibrium by using the currents in the LAs as feedback. Ideally, the variable mover mass of the IEA is levitated only by the reluctance force $F_{EPM}(t)$ and the Lorentz in a desired mover position without power consumption.

For the concept design of the IEA, a maximum load of 1 kg is targeted. The LAs levitate the mover in the desired position and the EPM compensates gravity, such that a maximum Lorentz and EPM force of about 10 N is required. The range of high precision positioning systems are typically within a few millimeters, hence a range of 4 mm is targeted [21]. Providing sub-micro-meter resolution, the IEA is applicable for precision measurement systems [6]. A positioning bandwidth of 100 Hz is targeted to attenuate low frequent disturbance forces. The targeted specifications are summarized in Tab. I.

TABLE I: Targeted specifications.

Position range	4 mm
Lorentz force	10 N
Static gravity compensation force at 1 mm	10 N
Position control bandwidth	100 Hz
Position control resolution	< 1 µm

III. System Design and Modeling

A. Mechanical system design

The mechanical design of the IEA can be separated into a stator and a mover, as shown in Fig. 3. The stator consists of a cylindrical NdFeB and an AlNiCo magnet, which is enveloped by the magnetization coil. Moreover, it includes two ferromagnetic yokes guiding the magnetic flux (i) of the EPM and (ii) of the permanent magnets for the LAs. For a compact design, the LAs are integrated into the yokes of the EPM, which is further discussed in Section III-C. To enable dynamic operation, the mover is comprised of lightweight parts, including the the Lorentz coils and the ferromagnetic yoke for the EPM. The supporting parts are required to be non-ferromagnetic to avoid disturbing parallel reluctances. In order to prevent magnetic saturation, all yokes are designed using a finite element analysis (FEA) tool (Maxwell 3D, Ansys Inc., USA).

The mover position is parametrized by the distances d_1 and d_2 with respect to each yoke part and is combined to the vectorial mover position $\boldsymbol{d} = \begin{bmatrix} d_1 & d_2 \end{bmatrix}^T$. Considering the coordinate system and the distance l_{sens} in Fig. 3, the mover

Post-print version of the article: A. Pechhacker, D. Wertjanz, E. Csencsics, and G. Schitter, "Integrated electromagnetic actuator with adaptable zero power gravity compensation," *IEEE Transactions on Industrial Electronics*, Early Access, 2023. DOI: 10.1109/TIE.2023.3288176

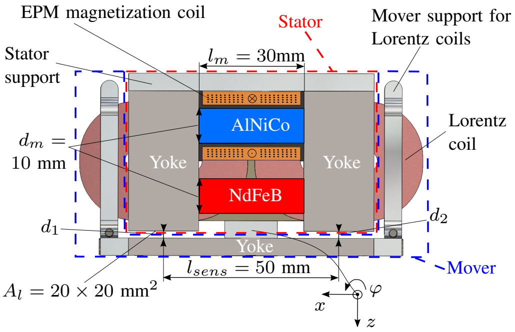

Fig. 3: Cross-section of the IEA design. The stator consists of two yokes, the NdFeB and AlNiCo magnet with the magnetization coil. The mover combines the yoke for the EPM and the Lorentz coils.

position can be transformed to a translational and rotational displacement:

$$z = \frac{d_1 + d_2}{2}, \qquad \varphi = \arctan\left(\frac{d_1 - d_2}{l_{sens}}\right). \tag{1}$$

The two integrated LAs allow the control of the two DoFs mover position. Based on the positioning range defined in Section II, the maximum rotation results to $\varphi_{max} = 3°$ with Eq. (1).

B. EPM design

Magnetostatic FEAs are used to design the EPM in order to meet the targeted requirements from Section II. Using the actuator dimensions indicated in Fig. 3, simulations are performed for parallel mover positions ($\varphi = 0°$) with the semi-hardmagnetic AlNiCo5 (grade LNG40) and the hardmagnetic NdFeB (grade N38) materials. The on state of the EPM with the AlNiCo and the NdFeB material magnetized in the same direction represents the maximum force of about 18N at $\boldsymbol{d} = [1\,\text{mm}\ 1\,\text{mm}]^T$. The anti-parallel magnetization of the AlNiCo and NdFeB magnet with no observable compensation force, defines the off sate. The EPM design intentionally exceeds the targeted specifications to have margins for manufacturing tolerances and differing magnetic properties.

To determine the requirements for the power electronics supplying the magnetization coil, the magnetization current i_{EPM} is calculated for the EPM transition between on and off state. Currents of $i_{EPM}^{off} \leq i_{EPM}^{tune} \leq i_{EPM}^{on}$ provide the seamless magnetization of the AlNiCo material. This enables the adaptation of the EPM reluctance force into a tuned state between the maximum and minimum force. Using Ampere's law and limiting the mover position to the translational DoF z (i.e. $\varphi = 0°$) yields

$$N_{EPM} i_{EPM} = 2H_l z + H_{Al} l_m, \tag{2}$$
$$N_{EPM} i_{EPM} = (H_{Al} - H_{Nd}) l_m, \tag{3}$$

with the turns of the magnetization coil N_{EPM}, the magnetization current i_{EPM} and the magnetic field strength in the air gaps H_l, the Alnico H_{Al}, and the NdFeB H_{Nd} magnet. For reasons of simplicity, the reluctance of the magnetic iron yokes are neglected in the design phase. Applying Gauss's law, yields

$$A_m\left(B_{Al} + B_{Nd}\right) = B_l A_l, \tag{4}$$

with the cross-section of the AlNiCo and NdFeB magnets A_m, the magnetic flux density in the AlNiCo magnet B_{Al}, in the NdFeB magnet B_{Nd} and in the air gap B_l. Due to the high coercivity of NdFeB, the B/H relation is approximated by a linear expression

$$B_{Nd} = B_r + \mu_0 H_{Nd}, \tag{5}$$

with the remanence B_r. The relation between magnetic flux and field in the air gap is given by

$$B_l = \mu_0 H_l. \tag{6}$$

Considering the saturation of AlNiCo5 magnets at about $H_{sat} = 150\,\text{kA/m}$ and $B_{sat} = 1.5\,\text{T}$ [22], the EPM is switched on by magnetically saturating the AlNiCo material in the same direction as the NdFeB magnetization and switched off with the magnetic saturation in the anti-parallel direction. By substituting $H_{Al} = \pm H_{sat}$, $B_{Al} = \pm B_{sat}$ in Eq. (2) - (6), the analytical result for the EPM switching current results to

$$i_{EPM} = \frac{2z l_m A_m (B_r \pm \mu_0 H_{sat} \pm B_{sat}) + H_{sat} l_m^2 A_l \mu_0}{N_{EPM}\mu_0 (A_l l_m + 2A_m z)}. \tag{7}$$

Eq. (7) is evaluated with the parameters from Fig. 3 and Section IV-A for $z = 0$ to $4\,\text{mm}$. The results are shown in Tab. II. By obtaining the numerical results, a dependency of the magnetization current based on the switching direction is observable. This dependency is caused by the remanence of the NdFeB magnet B_r, resulting in smaller magnetization currents for off-switching.

TABLE II: Analytical results of the EPM magnetization current for the transitions between on and off state.

z / mm	i_{EPM}^{on} / A	i_{EPM}^{off} / A
0	10.00	−10
1	11.89	−10.17
2	13.72	−10.34
3	15.51	−10.50
4	17.26	−10.66

As expected, the maximum switching current is required at 4 mm and the minimum at 0 mm (no air gap). The FEA reveals transient attraction forces of up to 72 N at $z = 0.5\,\text{mm}$ for on-switching. This transient force is caused by the increased magnetic flux in the air gaps while the magnetizing current pulses i_{EPM}. A force acting on the mover with its inertia yields a position error, which is be stabilized by the position control to remain in a floating position while the EPM is tuned. For off-switching, the simulation results show maximum attraction forces of 4 N at $z = 0.5\,\text{mm}$. As previously mentioned the remanence of the NdFeB magnet supports the off switching, reducing the amplitude of the magnetizing pulse to turn off the EPM and the related magnetic flux is mainly closing over the NdFeB magnet.

Post-print version of the article: A. Pechhacker, D. Wertjanz, E. Csencsics, and G. Schitter, "Integrated electromagnetic actuator with adaptable zero power gravity compensation," *IEEE Transactions on Industrial Electronics*, Early Access, 2023. DOI: 10.1109/TIE.2023.3288176

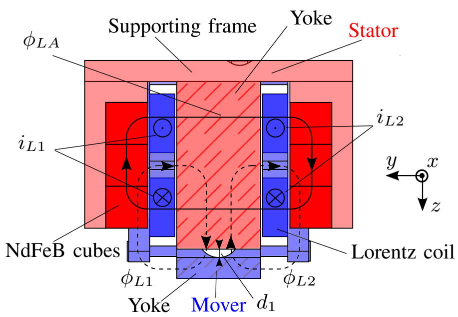

Fig. 4: Cross-section of the Lorentz actuator with the magnetic fluxes ϕ_{LA}, ϕ_{L1} and ϕ_{L2}, resulting from the NdFeB magnets and the currents in the Lorentz coils. The mover is marked in blue, the stator in red and the yokes are hatched.

C. Integrated Lorentz actuator

The EPM force attracts the mover with its negative stiffness in the air gaps d_1 and d_2, which destabilizes the mover position in two DoFs. To stabilize the mover at the desired position $\boldsymbol{d}$ with a fully actuated approach, two LAs are used. The magnetic flux density in the air gap for the Lorentz coils is obtained by 10 mm magnet cubes (NdFeB ,grade N48), which are aligned in a Halbach array on both sides of each yoke. The magnetic fluxes of a LA in the cross-section of a yoke are shown in Fig. 4. ϕ_{LA} is the magnetic flux provided by the magnet cubes and i_{L1} and i_{L2} are the currents in the Lorentz coils with $N_{LA} = 300$ turns. ϕ_{L1} and ϕ_{L2} indicate the fluxes generated by the currents in the Lorentz coils, which travel over the mover. These fluxes yield an additional reluctance force on the mover. Due to the symmetric distribution of the Lorentz coils in two equal parts aligned on both sides of the yokes, the fluxes cancel each other, if the Lorentz coils guide equal currents ($i_{L1} = i_{L2}$). In this way, the electromagnetic decoupling of the Lorentz and reluctance force is achieved, which can be ensured by connecting the LA coils of each yoke in series.

To achieve zero-stiffness actuation in the range of the targeted specifications, the Lorentz coils are designed with 4 mm coil overhung. Based on simulative maximization of the motor constant k_m, a Lorentz coil width of 6 mm is chosen. The FEA result of the LAs verify a linear model for the Lorentz force

$$F_{LA} = k_m i_{LA} \tag{8}$$

with a motor constant $k_m = 9.95\,\mathrm{N/A}$ for one of both identical LAs.

D. Position sensor system

The mover position of the designed IEA is required to be stabilized in two DoFs via its LAs. For feedback control of the mover position $\boldsymbol{d}$, two displacement sensors are required. To actuate and measure the mover position at the same location, the position sensors are aligned to directly measure the distances d_1 and d_2, providing the desirable actuator-sensor-collocation [23]. Due to a reasonable range, resolution and bandwidth optical proximity sensors are well suited for this task.

IV. System Implementation

In order to verify the simulation results and to evaluate the actuator performance, a prototype of the IEA is implemented in an experimental setup.

A. Integrated electromagnetic actuator

Figure 5a shows the fully assembled prototype of the IEA with the CNC machined supporting parts from AL6061 and the S235JR steel yokes. A copper wire with a diameter of 0.4 mm is used for the magnetization coil with $N_{EPM} = 450$ turns. The magnetization coil, wounded around the AlNiCo magnet, has a resistance of $R_{EPM} = 3.22\,\Omega$ and an inductance of $L_{EPM} = 1.99\,\mathrm{mH}$ at 1 kHz. One Lorentz coil, which is the series connection of two coil parts, have a resistance of $R_{LA} = 7.3\,\Omega$ and an inductance of $L_{LA} = 5.40\,\mathrm{mH}$ at 1 kHz. The mover and stator of the prototype have a weight of $m_{\text{mover}} = 245\,\mathrm{g}$ and $m_{\text{stator}} = 580\,\mathrm{g}$, respectively.

The LAs are driven by custom-made amplifiers with analog proportional-integral (PI) current controllers, enabling a bandwidth of 20 kHz and a maximum current of 1.99 mH. The motor constant k_m of each LA is measured with a force sensor (K3D500N, ME-Meßsysteme, Germany). The mean motor constant k_m in the range of 4 mm is determined to be 9.65 N/A for both LAs, which is in good accordance to the simulative result of 9.95 N/A.

B. Prototype system

Two optical proximity sensors (TCND5000, Vishay, USA) with custom-made readout electronics are used to measure the positions d_1 and d_2, enabling a bandwidth of >10 kHz and a resolution of 200 nm. The position sensors are aligned at the bottom side of the mover to minimize thermal impact of the LAs, visible in Fig. 5a.

The magnetic flux adaptation of the EPM requires bi-directional, current pulses in the magnetization coil. A common approach to magnetize permanent magnets are capacitive discharge magnetizers [24]. Therefore, a custom-made pulse generator based on a capacitive discharge magnetizer in combination with a IGBT full bridge with a calibrated current monitor is implemented, providing bi-directional current pulses i_{EPM} up to 80 A. The rapid prototyping system uses an industrial EtherCAT bus coupler (EK1100, Beckhoff Automation GmbH & Co. KG, Germany) with various analog and digital I/O-cards to control the prototype and acquire the measurement data. The TwinCAT3 development tool enables the real-time position control and EPM control with a Matlab/Simulink model. A sample frequency of 40 kHz is set and a time delay of $\tau_d = 100\,\mu\mathrm{s}$ is identified, which limits the bandwidth of the subsequent position control design and the accuracy of the magnetizing current pulses.

Post-print version of the article: A. Pechhacker, D. Wertjanz, E. Csencsics, and G. Schitter, "Integrated electromagnetic actuator with adaptable zero power gravity compensation," *IEEE Transactions on Industrial Electronics*, Early Access, 2023. DOI: 10.1109/TIE.2023.3288176

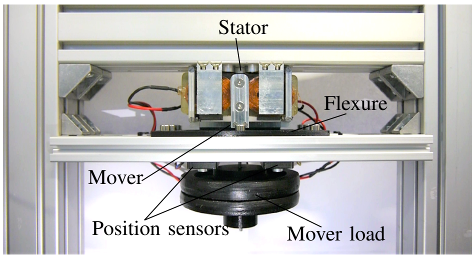

(a) Experimental setup overview.

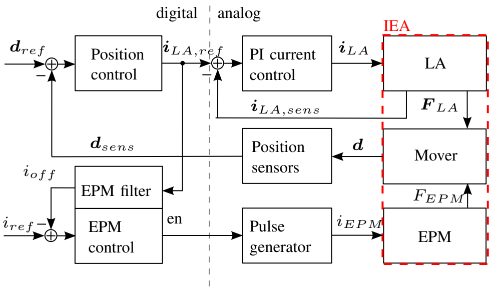

(b) Block diagram

Fig. 5: Experimental setup. a) shows the loaded actuator prototype vertically mounted to an aluminium profile structure. b) illustrates the architecture of the system components.

C. Experimental setup overview

The experimental setup consists of the vertically mounted prototype with the load connected to the center of the mover, which is shown in Fig. 5a. The mover load mass can be varied by adapting the number of the $0.5\,\mathrm{kg}$ weight plates. A guidance flexure with a vertical stiffness of $k_f = 920\,\mathrm{N/m}$ is connected to the mover to ensures the correct placement of the mover in the non-stabilized DoFs.

Figure 5b schematically illustrates the architecture of the system components in a block diagram. The inner PI current control loop for the LAs is implemented with an analog power circuit and the outer position control runs on the rapid prototyping system. Bold symbols in Fig. 5b, represent the two DoFs of the position control and the current controllers for the two LAs. The pulse generator applies current pulses with desired peak values, which are achieved by variable pulse lengths of the enable signal *en*, to the magnetization coil to tune the EPM force.

V. System Analysis and Control Design

A. Analysis of the EPM

To verify the magnetostatic FEA results of the EPM, the displacement-dependent force in a parallel mover position, i.e. $\varphi = 0°$, is acquired with a force sensor (K3D500N, ME-Meßsysteme, Germany) in the fully on/off-switched state. Additionally, the flux density in one air gap is measured with a Gauß-meter (GM08, Hirst Magnetics, UK) and a $0.6\,\mathrm{mm}$ transversal probe (TP002SP0.6, Hirst Magnetics, UK). The flux density B_l is assumed to be homogeneous in the air gap

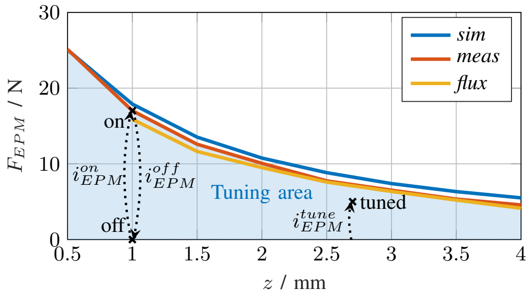

Fig. 6: The displacement-dependent EPM force obtained in the on state by the FEA *sim* (blue), the force measurement *meas* (red) and the calculation via the measured flux density in the air gap *flux* (yellow). The variable EPM force is marked with the tuning area between on and off state.

and the leakage flux is neglected, resulting a reluctance force of

$$F_{EPM} = \frac{B_l^2 A_l}{\mu_0} \quad . \tag{9}$$

The EPM is fully switched on/off with current pulses of $|i_{EPM}| > 25\,\mathrm{A}$ in every position, well exceeding the minimally required switching currents in Tab. II to ensure full magnetization of the AlNiCo magnet in both directions. Figure 6 shows the results of the force measurement (orange), the force calculated analytically using Eq. (9) with the measured flux density B_l (yellow) and the force obtained by the simulative FEA (blue). The EPM does not provide any significant remanence or static force in the off state. The measurements of the switched on EPM reveal a maximum force of $25\,\mathrm{N}$ at $z = 0.5\,\mathrm{mm}$, which is in good accordance with the simulative FEA results. For increasing air gap lengths, the FEA reveals higher forces in comparison to the measurements, which may be caused by differing coercivities of the AlNiCo5 in the FEA and the prototype.

The adaptation of the EPM force requires current pulses applied to the magnetization coil with variable amplitudes in the magnetization coil. These current pulses are obtained by constant voltage steps with certain pulse lengths, resulting in variable magnetizing peak currents $\hat{i}_{EPM}$. The amplitude of the voltage steps is set to $100\,\mathrm{V}$ by considering the trade-off between shorter pulse lengths, for reasons of energy efficiency and tuning dynamics, and longer pulse lengths for higher accuracy of the peak currents, limited by the sample frequency of the rapid prototyping system. As an example, the measured relation between the peak current and the resulting stationary force generated by the EPM when starting from the initial off state at $z = 1\,\mathrm{mm}$ is shown in Fig. 7 (left). The EPM force increases with higher current pulses till the AlNiCo material is fully magnetized and the EPM reaches the maximum force. Higher current pulses than the analytical result for the on switching i^{on}_{EPM}, from Tab. II, demonstrate only minor increase of the EPM force, verifying the analytical model.

Additionally, the magnetization currents for each measurement are shown in Fig. 7 (right). The EPM's non-linear mag-

Post-print version of the article: A. Pechhacker, D. Wertjanz, E. Csencsics, and G. Schitter, "Integrated electromagnetic actuator with adaptable zero power gravity compensation," *IEEE Transactions on Industrial Electronics*, Early Access, 2023. DOI: 10.1109/TIE.2023.3288176

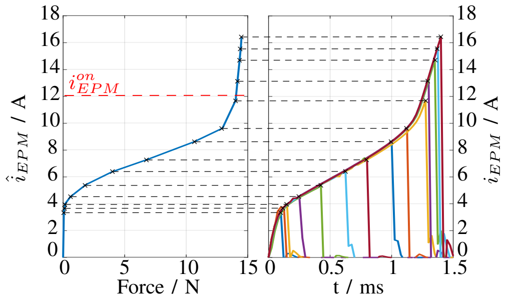

Fig. 7: EPM tuning process. (left) characterization of stationary tunable EPM force depending on the magnetizing peak current. (right) magnetizing currents measured while the EPM force tuning. The referring data points are connected with dashed lines.

netic properties yield a non-linear magnetization inductance, observable by the variable current slope with the AlNiCo material changing its magnetization. Summing up, the force can be adapted by magnetization current pulses with variable peak values. This relation is dependent on the mover position and the magnetization direction, as discussed in Section III-B.

B. Position control

Based on the unloaded system with disabled gravity compensation, a robust SISO position control is designed for the two DoFs LA to stabilize the mover position $\boldsymbol{d}$. Due to the symmetric system design, the plant for each DoF d_1/i_{LA1} and d_2/i_{LA2} can be approximated with a mass-spring-damper model

$$P(s) = \frac{k_m}{\frac{1}{2}(ms^2 + cs + k)} e^{-\tau_d s} \; , \tag{10}$$

with the mass $m = m_{\text{mover}} = 245\,\text{g}$, the stiffness of the guidance flexure $k = k_f = 920\text{N/m}$, the damping $c = 2.45\,\text{N s/m}$ and the time delay of the rapid prototyping system τ_d. The tamed PID control

$$C_{PID} = k_P \frac{1 + s/\omega_D}{1 + s/\omega_t} + \frac{k_I}{s} \tag{11}$$

with the parameters $\omega_D = 1.047 \cdot 10^2\text{rad/s}$, $\omega_t = 1.046 \cdot 10^3\text{rad/s}$, $k_P = 4.131 \cdot 10^2$ and $k_I = 1.298 \cdot 10^4\text{rad/s}$ is synthesized for a cross-over frequency of 75 Hz in a loop-shaping approach [7], resulting in a phase and gain margin of 48° and 26 dB, respectively.
Considering the time-variant system behaviour caused by a variable load mass $m(t) = m_{\text{mover}} + m_{\text{load}}(t)$ and the system controlled on the mass-line, the crossover frequency of the open-loop transfer function may vary. By limiting the maximum load mass to 1.5 kg, the crossover frequency is in the range from 75 Hz to 17 Hz. The minimum phase margin of 10° is obtained for the maximum load mass due to the shifted crossover frequency. The gravity compensation by the magnetization of the EPM introduces a variable stiffness $k(t) = k_f - k_{EPM}(t)$ with $k_{EPM}(t) \geq 0$ to the positioning system, as observable by comparing the slopes between on and off state of the EPM force in Fig. 6. Since the system is controlled on the mass-line, the phase- and gain margin are only depending on the load mass, regardless of magnetization of the EPM. To evaluate the stabilizing position control, the complementary sensitivity function of the Lorentz actuated loop is identified, shown in Fig. 8. The bandwidth of the unloaded system (T_{0kg}) is 138 Hz and is decreased to 28 Hz for a load of 1.5 kg ($T_{1.5kg}$). The gravity compensated measurement (T_{gc}) is carried out with a load of 1 kg and the reluctance force of the EPM is adapted according to the gravitational force acting on the mover mass, that $F_{EPM} = F_G$. The measurement of T_{gc} reveals a gain peak at 17 Hz, caused by the changed system behaviour, originating from the adaptation of the EPM force F_{EPM}.

C. EPM control

The reluctance force of the EPM needs to be adapted by magnetization current pulses to obtain the force equilibrium $F_{EPM}(t) = F_G(t)$, enabling the zero power gravity compensation. The offset current of the LAs

$$i_{off}(t) = \frac{F_G(t) - F_{EPM}(t)}{2k_m} = \frac{F_{residual}(t)}{2k_m} \quad , \tag{12}$$

indicate the deviation between the gravitational F_G and EPM force F_{EPM}. By increasing the EPM force of the residual force, ideally no Lorentz force is needed to levitate the mover mass, yielding no currents in the LAs. The EPM filter determines the offset current i_{off} by averaging the Lorentz currents i_{LA1} and i_{LA2}, which evaluates the Lorentz currents acting in the vertical DoF (i.e. $\varphi = 0°$). To attenuate high frequent disturbances, a moving average filter with a window length of 1000 is used to implement a FIR low-pass filter. Additionally, the values of i_{LA1} and i_{LA2} are discarded for 20 ms beginning at each magnetizing pulse to reduce the impact of the the previously mentioned transient disturbance force. To avoid deviations due to unmodelled system properties (e.g. eddy currents, temperature dependent material properties), a robust, iterative approach is applied. Assuming a sufficiently slow change rate of the variable mass $m(t)$ and the mover position $\boldsymbol{d}(t)$ in comparison the EPM control bandwidth, the control task can be treated as an optimization problem [25]. The power dissipation $P_{LA}(\hat{i}_{EPM})$ of the LAs

$$\min_{\hat{i}_{EPM} \in [i_{EPM}^{off}; i_{EPM}^{on}]} P_{LA}(\hat{i}_{EPM}) = 2 i_{off}(\hat{i}_{EPM})^2 R_{LA} \tag{13}$$

is the cost function, which needs to be minimized. The optimization problem is solved using a local search algorithm. Based on the sign of i_{off}, the algorithm incrementally increases the current pulses i_{EPM} by 0.1 A until the termination condition $|i_{off}| \leq i_{term}$ is fulfilled. The algorithm is restarted, if the termination condition is violated. Due to the cascaded control design, the cycle time of the outer EPM control loop $t_{EPM} = 100\,\text{ms}$ is defined around 10 times slower than the inner position control loop. The termination offset current $i_{term} = 10\,\text{mA}$ is defined by the minimum value, which shows a robust and permanent fulfilment of the termination condition in the experimental setup.

Post-print version of the article: A. Pechhacker, D. Wertjanz, E. Csencsics, and G. Schitter, “Integrated electromagnetic actuator with adaptable zero power gravity compensation,” *IEEE Transactions on Industrial Electronics*, Early Access, 2023. DOI: 10.1109/TIE.2023.3288176

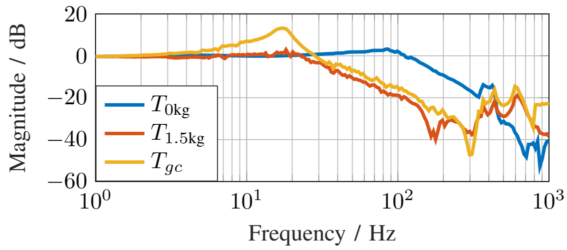

Fig. 8: Measured complementary sensitivity function of the unloaded system (T_{0kg}), the 1.5 kg loaded system ($T_{1.5kg}$) and the loaded system with active gravity compensation $F_{EPM} = F_G$ (T_{gc}).

VI. Evaluation of System Performance

In order to verify the performance of the experimental system, the influence of the variable load and the gravity compensation on the stationary positioning error is evaluated. Additionally, the dynamic behaviour and static power reduction regarding the EPM is evaluated.

The dynamic behaviour of the gravity compensation mechanism is evaluated with a load of 1.5 kg in the stabilized reference position $\boldsymbol{d}_{ref} = [1\,\text{mm}\;\;1\,\text{mm}]^T$ and the initially switched off EPM. By enabling the EPM control at 1 s, the system response for a mover mass step $m(t)$ of $m_{mover} + 1.5\,\text{kg} = 1.75\,\text{kg}$ is evaluated. Figure 9 shows the mover position $\boldsymbol{d}$, the offset current in the Lorentz coils i_{off}, the magnetic flux density in the air gap B_l and the magnetizing current pulses i_{EPM}. At the beginning the mover is levitated by the offset current $i_{off} = 1A$ in the LAs. The EPM control is enabled at $t = 1\,\text{s}$ and starts to increases the current pulses i_{EPM} due to the violation of the termination condition. These current pulses increase the magnetic flux density B_l and the resulting EPM force, reducing the offset current i_{off}. The termination condition is fulfilled at 5.5 s for the fist time while a maximum position control error of around 19 µm can be observed in both DoFs due to the transient disturbance force of the magnetizing pulses i_{EPM}. The EPM control undershoots the offset current reference of 0 A and violates the termination condition, whereupon the EPM control algorithm is restarted to apply linearly increasing magnetizing pulses in reversed direction. The transient disturbance force of magnetizing pulses to decrease the EPM force are smaller in comparison to the pulses to increase the EPM force, as discussed in Section III-B, such that the position control is able to reduce the error. The gravity compensation process finishes after 7.5 s and the offset current i_{off} remains permanently in the limits of the termination condition, verifying the adaptable gravity compensation mechanism of the designed IEA. A final magnetic flux density of $B_l = 232\,\text{mT}$ is observable, resulting in a reluctance force of 17.1 N with Eq. (9), corresponding with the compensated gravitational force $F_G = mg = 17.1\,\text{N}$. The variation of the magnetization current amplitudes are caused by the delay time and the sample rate of the rapid prototyping system. By dividing the compensated gravitational force of about F_G by the duration of the compensating process

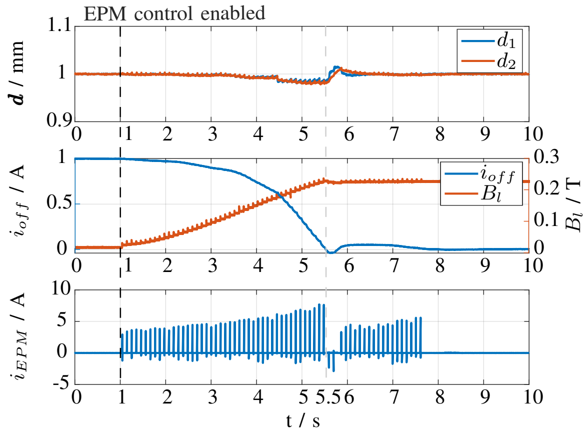

Fig. 9: The EPM control dynamically tunes the force to compensate a 1.5 kg load. At 1 s the EPM control is enabled and the subsequent system behaviour of the mover position $\boldsymbol{d}$, the offset current in the LAs i_{off}, the magnetic flux density in the air gap B_l and the current in the magnetizing coil i_{EPM} are measured.

of 6.5 s, the tuning rate of the EPM control is determined to 2.63 N/s.

Based on the termination condition with the previously experimentally defined termination offset current $i_{term} = 10\,\text{mA}$, the upper border for the power consumption for the compensated state is given by

$$P_{comp} \leq 2 i_{LA}^2 R_{LA} = 1.46\,\text{mW}, \tag{14}$$

with the resistance of the LA coils R_{LA}. The power consumption of the uncompensated state with 1.5 kg load is determined by the measured offset current with the switched off EPM $i_{off} = 1\text{A}$, resulting in

$$P_{uncomp} = 2 i_{term}^2 R_{LA} = 16.1\,\text{W}. \tag{15}$$

Comparing these two values, the static power dissipation is reduced by at least four orders of magnitude with the adaptable gravity compensation in relation to the purely LA-based positioning system. The overall energy dissipation of the experimental setup to tune the EPM force, shown in Fig. 9, is 3 J. Considering the power savings in the compensated state, the proposed system has a higher energy efficiency in comparison to the purely LA-based positioning system after remaining 190 ms in a constant position.

Lastly, the accuracy of the the position control is evaluated with no load and 1.5 kg load in a parallel mover position $\boldsymbol{d}_{ref} = [1\,\text{mm}\;\;1\,\text{mm}]^T$. The RMS positioning errors in the gravitationally uncompensated ($e_1 = 352\,\text{nm}$, $e_2 = 447\,\text{nm}$) and compensated state ($e_1 = 337\,\text{nm}$, $e_2 = 411\,\text{nm}$) of the positions d_1 and d_2 are determined. All test cases show a positioning error near the resolution of the positioning sensors, verifying the targeted sub-micro-meter resolution of the position control.

Post-print version of the article: A. Pechhacker, D. Wertjanz, E. Csencsics, and G. Schitter, "Integrated electromagnetic actuator with adaptable zero power gravity compensation," *IEEE Transactions on Industrial Electronics*, Early Access, 2023. DOI: 10.1109/TIE.2023.3288176

In summary, the designed IEA provides a seamlessly tunable force to actively compensate the gravitational force of a variable mass at a desired position, enabling a experimentally verified power reduction of at least four orders of magnitude, compared to the purely LA-based positioning system.

VII. Conclusion

An integrated electromagnetic actuator is presented, which is capable of zero power gravity compensation for variable masses at a desired position. The design combines a variable reluctance actuator with an EPM to compensate quasi-static gravitational forces, as well as Lorentz actuators to stabilize two DoFs of the mover in a desired position. In contrast to the state-of-the-art principles, the novel zero power gravity compensation mechanism seamlessly tunes the magnetization of the EPM while the mover remains in a constant position. A PID controlled two DoFs LA achieves a load-dependent position control bandwidth of up to $138\,\mathrm{Hz}$ and sub-micro-meter accuracy. Using the offset currents in the Lorentz actuators as feedback for the EPM control, the quasi-static reluctance force is seamlessly tuned in a range between 0 and $25\,\mathrm{N}$ by a local search algorithm. Measurement results verify a reduction of the power consumption by at least four orders of magnitude in the experimental setup of the integrated electromagnetic actuator with respect to the purely LA-based positioning system. A tuning rate of $2.6\,\mathrm{N/s}$ of the gravity compensation mechanism is experimentally identified for a mass step of $1.75\,\mathrm{kg}$, while remaining in a magnetically levitating position. The evaluated sub-micro-meter positioning resolution in a stationary state of the system proves the utilization for high-precision application, such as vibration isolation systems or positioning systems. Future work includes research towards an optimal EPM and position control design to improve the dynamic system response.

References

[1] T.-F. Yao, A. Duenner, and M. Cullinan, "In-line dimensional metrology in nanomanufacturing systems enabled by a passive semiconductor wafer alignment mechanism," *Journal of Micro and Nano-Manufacturing*, vol. 5, no. 1, 2016.

[2] H. Zhang, B. Kou, Y. Jin, H. Zhang, and L. Zhang, "Research on a low stiffness passive magnetic levitation gravity compensation system with opposite stiffness cancellation," *IEEE Transactions on Magnetics*, vol. 50, no. 11, pp. 1–4, 2014.

[3] J.-P. Yonnet, "Permanent magnet bearings and couplings," *IEEE Transactions on Magnetics*, vol. 17, no. 1, pp. 1169–1173, 1981.

[4] T. Zhu, B. Cazzolato, W. S. Robertson, and A. Zander, "Vibration isolation using six degree-of-freedom quasi-zero stiffness magnetic levitation," *Journal of Sound and Vibration*, vol. 358, pp. 48–73, 2015.

[5] H. Song, Z. Liu, X. Chen, S. Liu, M. Zhang, and H. Lu, "Research on reactive power optimization and voltage control of power grid based on gravity energy storage technology," in *2022 International Conference on Computers, Information Processing and Advanced Education (CIPAE)*, IEEE, 2022.

[6] D. Wertjanz, T. Kern, E. Csencsics, and G. Schitter, "Bringing the lab to the fab: Robot-based inline measurement system for precise 3D surface inspection in vibrational environments," *IEEE Transactions on Industrial Electronics*, 2022.

[7] R. M. Schmidt, G. Schitter, A. Rankers, and J. van Eijk, *The design of high performance mechatronics : high-tech functionality by multidisciplinary system integration*. Amsterdam: Delft University Press, 2020.

[8] D. Wertjanz, E. Csencsics, J. Schlarp, and G. Schitter, "Design and control of a MAGLEV platform for positioning in arbitrary orientations," in *2020 IEEE/ASME International Conference on Advanced Intelligent Mechatronics (AIM)*, IEEE, 2020.

[9] D. B. Hiemstra, G. Parmar, and S. Awtar, "Performance tradeoffs posed by moving magnet actuators in flexure-based nanopositioning," *IEEE/ASME Transactions on Mechatronics*, vol. 19, no. 1, pp. 201–212, 2014.

[10] S. Hol, E. Lomonova, and A. Vandenput, "Design of a magnetic gravity compensation system," *Precision Engineering*, vol. 30, no. 3, pp. 265–273, 2006.

[11] R. Deng, "Integrated 6-dof lorentz actuator with gravity compensation for vibration isolation in in-line surface metrology," Ph.D. dissertation, Delft University of Technology, Delft, 2017.

[12] Y.-M. Choi, "A new magnetic bearing using halbach magnet arrays for a magnetic levitation stage," *Review of Scientific Instruments*, vol. 80, no. 4, p. 045 106, 2009.

[13] G. Stadler, E. Csencsics, S. Ito, and G. Schitter, "High precision hybrid reluctance actuator with integrated orientation independent zero power gravity compensation," *IEEE Transactions on Industrial Electronics*, vol. 69, no. 12, pp. 13 296–13 304, 2022.

[14] M. Raab, M. Hutter, A. Kazi, W. Schinkoethe, and B. Gundelsweiler, "Magnetically levitated linear drive using an active gravity compensation based on hybrid shape memory actuators," *IEEE/ASME Transactions on Mechatronics*, vol. 26, no. 3, pp. 1380–1391, 2021.

[15] A. Knaian, "Electropermanent magnetic connectors and actuators: Devices and their application in programmable matter," Ph.D. dissertation, Massachusetts Institute of Technology, Dept. of Electrical Engineering and Computer Science, Massachusetts, 2010.

[16] S. Qin, H. Zhang, Y. Mao, *et al.*, "Electropermanent magnet blank holder technique in sheet metal deep drawing," *The International Journal of Advanced Manufacturing Technology*, vol. 106, no. 11-12, pp. 5497–5507, 2020.

[17] C. Velez, L. P. Tatum, B. S. Herstein, C. P. Becker, and D. P. Arnold, "Batch-fabrication and characterization of miniaturized axisymmetric electropermanent magnets," *Journal of Physics: Conference Series*, vol. 1052, p. 012 045, 2018.

[18] A. Gholizadeh, S. Abbaslou, P. Xie, A. Knaian, and M. Javanmard, "Electronically actuated microfluidic valves with zero static-power consumption using electropermanent magnets," *Sensors and Actuators A: Physical*, vol. 296, pp. 316–323, 2019.

[19] P. Ward and D. Liu, "Design of a high capacity electro permanent magnetic adhesion for climbing robots," in *2012 IEEE International Conference on Robotics and Biomimetics (ROBIO)*, IEEE, 2012.

[20] T. Li, F. Chen, Z. Zhao, Q. Pei, Y. Tan, and Z. Zhou, "Hybrid data-driven optimization design of a layered six-dimensional FBG force/moment sensor with gravity self-compensation for orthopedic surgery robot," *IEEE Transactions on Industrial Electronics*, vol. 70, no. 8, pp. 8568–8579, 2023.

[21] S. Ito, S. Troppmair, B. Lindner, F. Cigarini, and G. Schitter, "Long-range fast nanopositioner using nonlinearities of hybrid reluctance actuator for energy efficiency," *IEEE Transactions on Industrial Electronics*, vol. 66, no. 4, pp. 3051–3059, 2019.

[22] P. Campbell and S. Al-Murshid, "A model of anisotropic alnico magnets for field computation," *IEEE Transactions on Magnetics*, vol. 18, no. 3, pp. 898–904, 1982.

[23] J. Sun, "Some observations on physical duality and colocation of structural control sensors and actuators," *Journal of Sound and Vibration*, vol. 194, no. 5, pp. 765–770, 1996.

[24] S. Chen, K. Huang, and F. Juang, "Improvement of a capacitor discharge impulse magnetizer circuit," in *The Fifth International Conference on Power Electronics and Drive Systems, 2003. PEDS.*, IEEE, 2003.

[25] I. Griva, *Linear and nonlinear optimization*. Society for Industrial and Applied Mathematics, 2008.

Post-print version of the article: A. Pechhacker, D. Wertjanz, E. Csencsics, and G. Schitter, "Integrated electromagnetic actuator with adaptable zero power gravity compensation," *IEEE Transactions on Industrial Electronics*, Early Access, 2023. DOI: 10.1109/TIE.2023.3288176

Alexander Pechhacker is doctoral researcher in the Advanced Mechatronic Systems group at the Automation and Control Institute (ACIN) at TU Wien, Vienna, Austria. He received an MSc degree in Electrical Engineering from TU Wien, Austria in 2022. His primary research interests are on high performance mechatronic systems design, electromagnetic actuator design and high precision position control.

Daniel Wertjanz is doctoral researcher at the Automation and Control Institute (ACIN) at TU Wien, Vienna, Austria. He received an MSc degree in Electrical Engineering from TU Wien in 2019. His primary research interests are on high performance mechatronic systems design, high precision motion control, and automated inline measurement systems.

Ernst Csencsics is assistant professor for Measurement Systems in the Advanced Mechatronic Systems group at the Automation and Control Institute (ACIN) of TU Wien. He received an MSc and a PhD degree (sub auspiciis) in Electrical Engineering from TU Vienna, Austria in 2014 and 2017, respectively. His primary research interests are on high performance mechatronic systems, the development of holistic methods for multidisciplinary system design and integration, opto-mechatronic measurement and imaging systems, precision engineering, and robot-based in-line measurement systems. He received the journal best paper award of IEEE/ASME Transactions on Mechatronics (2018) and the best student paper award at the American Control Conference (2016).

Georg Schitter is Professor for Advanced Mechatronic Systems at the Automation and Control Institute (ACIN) of TU Wien. He received an MSc in Electrical Engineering from TU Graz, Austria (2000) and an MSc and PhD degree from ETH Zurich, Switzerland (2004). His primary research interests are on high-performance mechatronic systems, particularly for applications in the high-tech industry, scientific instrumentation, and mechatronic imaging systems, such as AFM, scanning laser and LIDAR systems, telescope systems, adaptive optics, and lithography systems for semiconductor industry. He received the journal best paper award of IEEE/ASME Transactions on Mechatronics (2018), of the IFAC Mechatronics (2008-2010), of the Asian Journal of Control (2004-2005), and the 2013 IFAC Mechatronics Young Researcher Award. He served as an Associate Editor for IFAC Mechatronics, Control Engineering Practice, and for the IEEE Transactions on Mechatronics.

Post-print version of the article: A. Pechhacker, D. Wertjanz, E. Csencsics, and G. Schitter, "Integrated electromagnetic actuator with adaptable zero power gravity compensation," *IEEE Transactions on Industrial Electronics*, Early Access, 2023. DOI: 10.1109/TIE.2023.3288176